Electronic and magnetic structure of $R\mathrm{ScO}_3$ (R=Sm,Gd,Dy) from x-ray spectroscopies and first-principles calculations

M. Raekers,[1,*] K. Kuepper,[2,†] S. Bartkowski,[1] M. Prinz,[1] A. V. Postnikov,[3] K. Potzger,[2] S. Zhou,[2] A. Arulraj,[4] N. Stüßer,[4] R. Uecker,[5] W. L. Yang,[6] and M. Neumann[1,‡]

[1]*Department of Physics, University of Osnabrück, D-49069 Osnabrück, Germany*

[2]*Institute of Ion Beam Physics and Materials Research, Forschungszentrum Dresden-Rossendorf, P.O. Box 51 01 19, D-01314 Dresden, Germany*

[3]*Laboratoire de Physique des Milieux Denses, Unversité Paul Verlaine, 1 Boulevard Arago, F-57078 Metz, France*

[4]*Department of Magnetism, Hahn-Meitner-Institut, Berlin, Glienicker Strasse 100, 14109 Berlin, Germany*

[5]*Institute for Crystal Growth, Max-Born-Street 2, D-12489 Berlin, Germany*

[6]*Advanced Light Source, Lawrence Berkeley National Laboratory, Berkeley, California 94720, USA*

(Received 19 November 2008; revised manuscript received 28 January 2009; published 23 March 2009)

The electronic structures of SmScO_3, GdScO_3, and DyScO_3 are investigated by means of x-ray photoelectron spectroscopy, x-ray emission spectroscopy (XES), and x-ray absorption spectroscopy (XAS). A strong hybridization between Sc 3*d* and O 2*p* is found, and a contribution of the rare-earth 5*d* states to this hybridization is not excluded. The band gaps of the compounds are determined by combining XES and XAS measurements. For SmScO_3, GdScO_3, and DyScO_3 the band gaps were determined to be 5.6, 5.8, and 5.9 eV, respectively. Magnetization versus temperature measurements reveal antiferromagnetic coupling at 2.96 (SmScO_3), 2.61 (GdScO_3), and 3.10 K (DyScO_3). For DyScO_3 a Rietveld refinement of a 2 K neutron-diffraction data set gives the spin arrangement of Dy in the *Pbnm* structure (Shubnikov group: $Pb'n'm'$).

DOI: 10.1103/PhysRevB.79.125114 PACS number(s): 77.84.Bw, 32.30.Rj, 71.20.−b, 71.15.Mb

I. INTRODUCTION

Perovskites of the type RMO_3, where R^{3+} represents a trivalent rare-earth metal and M is a trivalent or mixed-valent transition-metal ion, exhibit an enormous variety of physical properties.[1] During the last decade the so-called manganites have attracted much attention due to their unusual magnetic transport phenomena resulting in the colossal magnetoresistance (CMR) effect.[2,3] These compounds are also promising candidates for various potential applications, e.g., for hard disk drive reading heads or in the rapidly growing field of magnetic random access memory (MRAM). On the other hand, ferroelectric perovskites such as KTaO_3, KNbO_3, LiNbO_3, or BaTiO_3 have been subjected to intense studies due to their unusual dielectric properties and the possibility to switch the electrical polarization.[4] This leads to the idea that information can be also stored using the electrical polarization state of a ferroelectric material (FeRAM).[5,6] A practical realization of such devices demands to prepare high quality thin films with thickness of the micron scale in order to operate switches at few volts whereas the coercive voltages in these materials are at the order of kV per centimeter. These materials may also be used in somewhat related applications mentioned above, such as the next-generation semiconductor components (to replace the SiO_2 gate dielectric). With the continued scaling of the gate oxide to below 2 nm, leakage currents due to tunneling became very high. Therefore it is necessary to increase the thickness of the gate dielectrics without reduction in the associated capacitance. This can be achieved with materials which exhibit a high dielectric constant k. Lucovsky *et al.*[7] found that increases in k are generally accompanied by decreases in the optical band gap E_g, the conduction-band offset energy with respect to Si E_B, and the effective electron tunneling mass m_{eff}.[7] Hence the adjustment of the electronic band structure plays an important role in tuning the high-k materials.[7] In the last years a number of high-k compounds were observed.[8] The ternary oxide scandates SmScO_3, GdScO_3, and DyScO_3 are promising candidates to serve as high-k dielectrics in future applications.[9,10] Furthermore these materials are utterly interesting substrates for the production of highly strained ferroelectric thin films. Thin ferroelectric films often show strong epitaxial strain effects, e.g., the change in critical temperatures, crystal structure, and thus ferroelectric properties as a consequence to the growth on a substrate with defects or different lattice parameters. These strains can deteriorate the required thin-film properties but also be used to control and optimize the desired ferroelectric properties if one finds a suitable high quality substrate. During the last few years the family of scandates such as SmScO_3, GdScO_3, or DyScO_3 has bridged the gap of suitable substrates, thus widening the scope for strain tailoring of the films and allowing to explore experimentally some of the desired predictions and properties.[6,11–13] Very recently it has been shown that $\mathrm{SrTiO}_3/\mathrm{DyScO}_3$ multilayers can be also used for modulation of the permittivity in terahertz range.[14]

Due to all the above-described experimental progress and potential applications, proper theoretical approaches to describe and predict the variety of properties in ferroelectric materials such as the scandates are highly desirable. Hence, these materials are subject to numerous first-principles studies for almost two decades now. Such calculations within density-functional theory (DFT) offer a very powerful possibility to describe the structural, magnetic, and electronic structures of ferroelectrics in deep detail. However, there are some known limitations and inaccuracies. In particular in presence of rare-earth 4*f* orbitals, the widely used local density approximation (LDA) and, to some extent, also the gen-

eralized gradient approximation (GGA) lead to a qualitatively incorrect description of the $4f$ energy placement. A related problem is that the structural properties, due to wrongly estimated localization of the $4f$ states, are often described improperly. There are a number of approaches in order to minimize or overcome these limitations. Some works include a Hubbard U parameter in order to consider the Coulomb repulsion between the highly localized $4f$ electrons. Some very recent works apply hybrid exchange functionals that combine fixed amounts of Hartree-Fock and LDA or GGA functionals to rare-earth oxides as CeO_2 or ferroelectric oxides such as $BaTiO_3$.[15,16]

Concerning the scandates, up to now only some electronic structure calculations for $DyScO_3$ have been reported.[17] From the experimental point of view only a few ultraviolet ellipsometry data, x-ray absorption spectroscopy (XAS) data, and a combination of internal photoemission and photoconductivity studies are available up to now.[7,18,19] However, in order to achieve a proper description of the electronic properties of rare-earth-based ferroelectric oxides (such as the scandates investigated here) a comparison with suitable experiments is of utmost importance. The techniques of x-ray photoelectron spectroscopy (XPS), XAS, and x-ray emission spectroscopy (XES) are powerful tools of unique precision in order to directly probe the total and partial densities of states (tDOS and pDOS, respectively) of ferroelectric materials.[20–22] Therefore we perform a detailed electronic structure investigation of $SmScO_3$, $GdScO_3$, and $DyScO_3$ by combining the complementary experimental techniques of XPS, XES, and XAS. We compare our experiments with first-principles electronic structure calculations. Furthermore we probe the magnetic structure of these samples by means of a superconducting quantum interference device (SQUID) and neutron powder diffraction.

II. EXPERIMENTAL AND THEORETICAL DETAILS

High quality $SmScO_3$, $GdScO_3$, and $DyScO_4$ single crystals were grown by the conventional Czochralski technique by Uecker *et al.*[23] The XAS and XES on these samples were performed at room temperature at beamline 8.0.1 at the Advanced Light Source, Berkeley, California, USA, using the soft x-ray fluorescence (SXF) end station of the University of Tennessee at Knoxville.[24] Linearly polarized light with polarization in the horizontal plane was incident on the sample whose surface was in the vertical plane. The emission was measured along the electric vector of the incident light in the horizontal plane, that is, at a scattering angle of 90°. This geometry minimizes diffuse elastic scattering from the surface since the Brewster angle in the soft x-ray range is usually very close to 45° so that the reflectivity for $\vec{p}$ light is very close to zero. The light was incident at 30° to the sample normal. Photons with an energy of 65–1400 eV were provided to the end station via a spherical 925 lines/mm grating monochromator. The rare-earth $4f \rightarrow 3d$, Sc $3d \rightarrow 2p$, and O $2p \rightarrow 1s$ XES were obtained with a 1500 lines/mm, 10-m-radius grating. The excitation energies for the x-ray emission (XE) spectra were set to 420.2 eV for the Sc $L_{2,3}$ edge and to 542.1 eV for the O K edge. The rare-earth $M_{4,5}$ edges were exited with 1141 (Sm), 1260 (Gd), and 1360 eV (Dy). Since the SXF detector cannot analyze photons with energies over 1000 eV, the latter spectra were recorded in second order of the spectrometer. The overall resolution of the beamline plus spectrometer was set to around 0.7 eV for the oxygen and scadium spectra and to around 1 eV for the rare-earth XES. The resolution can be obtained from the full width at half maximum (FWHM) of the corresponding elastic recombination peaks. Absorption was measured in total fluorescence yield with a channeltron. The entrance and exit slits were set to 40 μm resulting in an overall resolution of 0.4 eV.

The XPS valence bands (VBs) were recorded at the Department of Physics, University of Osnabrück, Germany, using a PHI 5600ci multitechnique spectrometer with monochromatic Al K_α=1486.6 eV radiation with FWHM =0.3 eV. The overall resolution of the spectrometer is 1.5% of the pass energy of the analyzer; 0.45 eV in the present case. The spectra were calibrated using the line of adsorbed carbon (C1s=285.0 eV) as a reference. Since $R\mathrm{ScO}_3$ (R =Sm,Gd,Sc) are insulators the sample surfaces were neutralized with a constant electron current from a soft electron gun during the measurements in order to compensate charging effects. For clean surfaces the samples were cleaved and measured in ultrahigh vacuum ($\approx 10^{-9}$ mbar).

Magnetization versus temperature measurements have been performed by means of a superconducting quantum interference device (SQUID) [Quantum Design magnetic property measurement system (MPMS) XL] at the Institute for Ion Beam Physics and Materials Research, Forschungszentrum Rossendorf.

Neutron powder diffraction of the compound $DyScO_3$ taken in a cylindrical vanadium container (diameter of 8mm) was recorded with the focusing diffractometer E6 at the Berlin Neutron Scattering Center (BENSC). The E6 diffractometer is equipped with a horizontally and vertically bent monochromator consisting of 105 pyrolytic graphite crystals ($20 \times 20 \times 2$ mm^3) mounted on a 15×7 matrix leading to a relatively high flux at the sample position. The incident wavelength was 2.442 Å. The data were collected at 2 and 300 K. The integration of the Debye-Scherrer rings measured on a two-dimensional (2D) detector resulted in intensity versus scattering angle 2Θ for each temperature. Crystal (magnetic) structure was further analyzed by Rietveld refinements employing the program GSAS.[25] An absorption correction for the cylindrical sample was carried out using GSAS for which a wavelength-dependent coefficient of 1.138 was used. A smoothly varying background was defined by extrapolating a fixed number of background points.

The electronic structure calculations were performed with the (linearized) full-potential augmented plane wave method—see, e.g., Ref. 26—of the density-functional theory, as implemented in the WIEN2K code.[27] For the exchange-correlation potential, we used the generalized gradient approximation in the form of Perdew-Burke-Ernzerhof.[28,29] In order to describe the effects of intra-atomic correlation beyond the conventional LDA or GGA treatment, we have taken into account the spin-orbit interaction and orbital-dependent potential, notably LDA+U (Ref. 30) (or rather GGA+U in our case), specifically in the "LDA+U(SIC)"

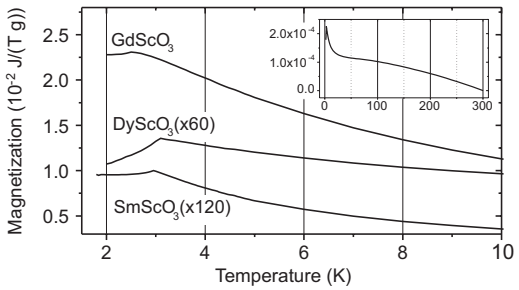

FIG. 1. *M-T* curves for $SmScO_3$, $GdScO_3$, and $DyScO_3$. The measurement was performed under an applied flux of $\mu_0 H=0.5$ T after cooling from 300 K in the same field. The magnification factor is indicated. The inset shows the high-temperature range for $DyScO_3$. The constant *M* offset at 300 K has been subtracted.

flavor of the WIEN2K implementation, with the correction added in the 4*f* shell of a rare earth. Even as the *U* and *J* values in the LDA+*U* formalism can be, in principle, estimated from first-principles calculations,[31] it is a more practical routine to use them as adjustable phenomenological parameters. In the present context, we were guided by the placement of occupied (majority-spin) *R* 4*f* states in the x-ray (photo)emission spectra, relative to other valence-band states. This sole criterion was, however, conflicting with the (experimentally founded) condition to have the band gap free from the minority-spin 4*f* states. In order to satisfy this second criterion, we preferred to use somehow elevated *U* values that resulted in a slightly overbonded majority-spin *R* 4*f* states. Our values of choice are $U=0.6$ Ry (8.2 eV) for Gd 4*f* and $U=0.8$ Ry (10.8 eV) for $SmScO_3$ and $DyScO_3$ as used in the following discussion (in part giving the reference to the results obtained with other *U* values as well). The *J* value was kept equal to 0.05 Ry (0.68 eV). The calculations were done in antiferromagnetic ordering which is explained in detail in Sec. III. These calculations are compared with experimental results of paramagnetic phase. In the comparison between the calculated tDOS and XPS results (Fig. 4) we present ferromagnetic calculations with $U=0.4$ Ry additionally to the antiferromagnetic calculation with $U=0.6$, 0.8 Ry. The rare-earth 4*f* states shift with the *U* value. The smaller *U* values give the right energy positions of occupied 4*f* states in the valence band but a too low (within the band gap) placement of their vacant counterparts. The nominal (as determined) crystal structure was used[32] (4 f.u./unit cell, all rare-earth positions being equivalent). The densities of states (DOSs) have been calculated with the *k* mesh $3\times2\times2$ over the Brillouin zone and have been smeared in the following figures for a more clear comparison with experimental spectra.

III. RESULTS AND DISCUSSION

A. Magnetic properties

First we want to discuss magnetic properties by means of magnetic measurements. Magnetization versus temperature SQUID measurements are presented in Fig. 1. We expected the materials $SmScO_3$, $GdScO_3$, and $DyScO_3$ to exhibit similar magnetic order such as the corresponding rare-earth (3+) oxides, i.e., antiferromagnetism at low Néel temperatures. E.g., for Dy_2O_3, this temperature is 1.2 K.[33] Note that discussions about the kind of magnetic ordering in $GdScO_3$ occurred in the past.[34] By our measurements basically the transition temperature of the substrates were obtained prior to neutron-diffraction measurement. The field-cooled *M-T* curves were measured at a field *H* determined by $\mu_0 H=0.5$ T. The field was applied parallel to the single crystal surface. Cusps typical for the onset of antiferromagnetic order occur at 2.96 ($SmScO_3$), 2.61 ($GdScO_3$), and 3.10 K ($DyScO_3$). While the former two substrates exhibit Brillouin-type behavior in the high-temperature range (not shown), the latter deviates significantly, exhibiting a large plateau (Fig. 1, inset). The peak for $GdScO_3$ is much broader than for the other samples. Moreover, $GdScO_3$ exhibits a much larger magnetization and thus behaves similar to Gd_2O_3.[34]

Exemplarily, $DyScO_3$ was investigated with respect to its microscopic magnetic structure by means of neutron diffraction. The room-temperature (300 K) data set could be indexed with an orthorhombic lattice with space group *Pbnm*. In the 2 K data set several peaks in addition to those present in the 300 K data were observed (Fig. 2). These peaks could be indexed with the propagation vector $k=0$ and are due to the antiferromagnetic arrangement of the spins of Dy in the low-temperature magnetic structure of $DyScO_3$. Of the four possible spin arrangements of the antiferromagnetic type only that with the magnetic group symmetry (Shubnikov groups: *Pbnm′* and *Pb′n′m′*) explains the presence of all the peaks of the 2 K data set. Symmetry analysis of the arrangement of the spin of Dy in the *Pbnm* structure of $DyScO_3$ indicates the following two possibilities. The first possibility is that the spin components of Dy belong to *G* mode with *y* component and *A* mode with *x* component (representation Γ_8) and in the second possibility *G* mode with *x* component and *A* mode with *y* component (representation Γ_5).[35] A Rietveld refinement of the 2 K neutron-diffraction data set gives a good fit only with the second possibility (Shubnikov group: *Pb′n′m′*). In Fig. 2 the crystal structure and the magnetic structure (spin arrangement) of $DyScO_3$ at 2 K are shown.

B. Calculated densities of states

Here we want to describe the calculated densities of states for three systems, obtained in true orthorhombic distorted perovskite structure (Fig. 3). Instead of the experimentally established noncollinear ferromagnetic structure depicted (for DyScO3) in Fig. 2, we considered its most straightforward collinear simplification, with spin moments of *R* centers set antiparallel between the nearest neighbors (both in the *ab* plane and along the *c* axis of Fig. 2). As the *R* magnetic moments are quite localized (and really negligible, below 0.01 μ_B, on Sc and O sites), the plotted partial DOS of the antiferromagnetic structure are practically indistinguishable from those in the ferromagnetic phase, which are used for comparison with room-temperature experiments.

It should be noted that we used the *U* value for the LDA+*U* calculation of 0.6 Ry for $GdScO_3$ and 0.8 Ry for $SmScO_3$ and $DyScO_3$. Its detailed tuning can be subjected to

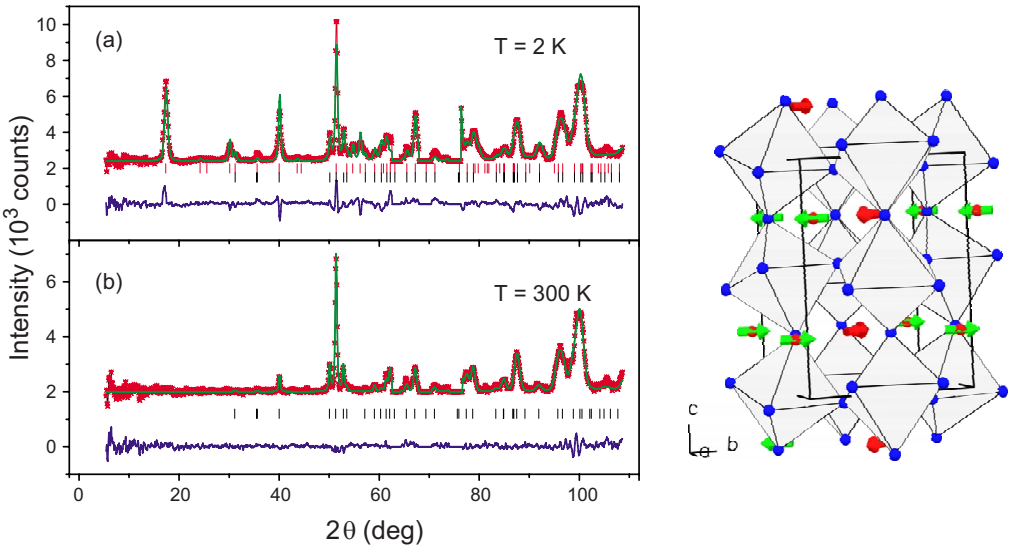

FIG. 2. (Color online) Neutron-diffraction and crystal (magnetic) structures of $DyScO_3$. Results of the Rietveld refinement of the (a) 2 and (b) 300 K neutron powder diffraction data of $DyScO_3$. The crystal and the magnetic structure (arrangement of arrows representing magnetic moments at Dy sites) is also shown.

careful analysis and argument. As stated above, we chose a compromise between the position of *R*4*f* states in the valence band and the need to the band gap free of the *R*4*f* states. Emphasizing a typically "semiempirical" character of the *U* values in practical calculations, we note that the examples are known where the *U* values have been evaluated over a range of rare-earth compounds. E.g., Larson *et al.*[36] cited a range of *U* values gradually varying from 7.47 (CeN) to 10.94 eV (LuN) in a row of rare-earth nitrides. Our values are close to those cited in Ref. 36, with a noticeable difference that we were primarily guided by the criteria named in Sec. II. Summarizing the results over different *U*, we note that the larger *U* values, understandably, move the (vacant) minority-spin 4*f* states out of the band gap, as desired.

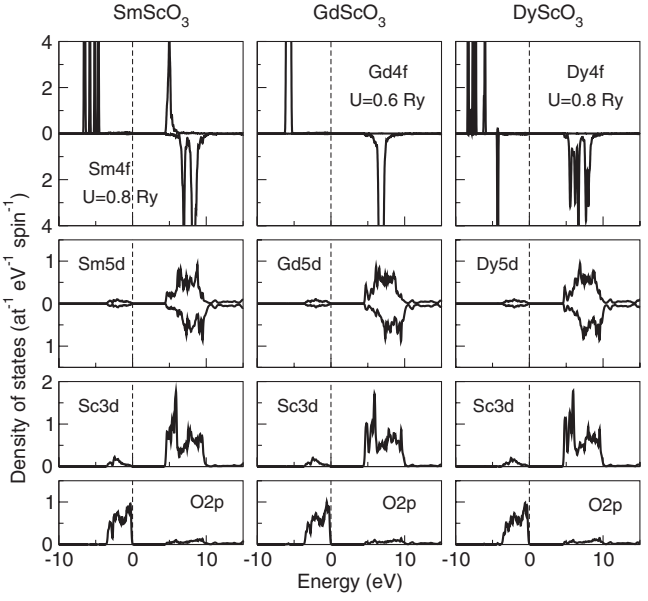

FIG. 3. Selected partial DOS in $SmScO_3$, $GdScO_3$, and $DyScO_3$. The zero of energy scale is set to the top of the valence band. For Sc 3*d* and O 2*p*, only one component of spin-resolved DOS is shown, which is indistinguishable from the other. Sc site is nonmagnetic by symmetry. O 2*p* stands for a mean value (per atom) over four inequivalent oxygen sites.

However, this happens at the expense of lowering the majority-spin Dy 4*f* well below its experimentally expected position. This problem illustrates the shortcoming and crudeness of the LDA+*U* approach: with a single tunable parameter it is difficult to accommodate the correct placement of 4*f* states relative to the valence band involving other atoms, and an introduction of further tunable *U* parameters (e.g., for Sc 3*d* and O 2*p* states) would sacrifice physical transparence.

With this in mind, we note in Fig. 3 that occupied *R*4*f* states are (intentionally) placed just below the valence band, which is formed predominantly by O 2*p*, with a small admixture of *R*5*d* and Sc 3*d* in the range between 0 and −3 eV. However, due to the orbital-dependent potential taken into account, the 4*f* peak remains narrow only for Gd (around −6 eV) with its half-filled shell, whereas for Sm (from −4.5 to −7 eV) and Dy (from −4.5 to −8.5 eV) it reveals a system of energy levels, yielding a non-negligible hybridization with the valence band (majority-spin states) and the conduction band (minority-spin states). Apart from the details of this hybridization, the Sc 3*d* partial DOS and the *R*5*d* DOS are almost identical throughout the three compounds (occupied: from 0 to −4 eV; unoccupied: 4.5–10 eV). For the comparison with the experimental data (Figs. 4–6) the Fermi level is shifted by ~−2.5 eV into the band gap. That the experimental Fermi level lies in the calculated gap can be due to a very small amount of defects.

C. X-ray spectroscopic experiments and discussion

Next we want to discuss the XPS valence-band spectra of $SmScO_3$, $GdScO_3$, and $DyScO_3$ (Fig. 4). The experiments are compared with the results of *ab initio* band-structure calculations, namely, the total density of states from a GGA

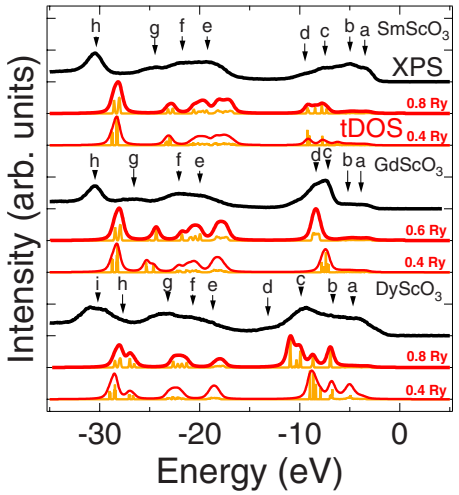

FIG. 4. (Color online) XPS valence bands (black thick lines) of $SmScO_3$ (top), $GdScO_3$ (middle), and $DyScO_3$ (bottom). The convoluted and weighted tDOS with different U values and the corresponding nonconvoluted tDOS are shown below the XPS. The calculations are shifted by −2.5 eV for comparison with experiment.

calculation which gives the best agreement with the experiment. The excitation (N-1 electrons) during the XPS process is not included in the calculations (N electrons). Hence the localized states at ∼−30 and ∼−20 eV in the calculations are located closer to the Fermi level than in the XPS measurement. Moreover, the multiplet effects are not included. The valence-band region is constituted by R 4f, 5p, 5d and Sc 3p, 3d, 4s and O 2p, 2s states. These states have different photoionization cross sections, which should be taken into account for weighting the corresponding DOS contributions to yield the simulated spectrum. Specifically, we took the relative photoionization cross-section values, corresponding to the excitation energy of 1486.6 eV, from Scofield.[37] The weights tabulated therein, which refer to each respective electronic shell as a whole, were normalized to a single electron and then multiplied with partial densities of states and with the number of atoms of each type in the unit cell, giving the calculated spectral intensity which is compared to the experiment. Then the calculated total density of states was convoluted with a 0.45 eV Gaussian and a 0.5 eV Lorentzian for experimental and lifetime broadening, respectively.

The valence-band region of $SmScO_3$ is composed of eight distinct features, a–h. Features a, b, and c at −3.5, −5.0, and −7.5 eV on the energy loss scale are followed by a shoulder d at −9.5 eV. The O 2p states are located from −3 to −5 eV, while the Sm 4f multiplet is found in features b, c, and d. The next group of features (e, f, and g) is located at −19.5, −21.5, and −24.5 eV. In this region the O 2s states take place around −23 eV and the Sm 5p multiplet reaches from −19 to −25 eV. At −30.5 eV feature h appears which corresponds to Sc 3p states. The experiment is very well reproduced by the calculation with U=0.4 Ry besides the intensities of Sm 4f multiplet features b, c, and d. For U =0.8 Ry the calculated Sm 4f states are less splitted and appear too far away from the Fermi level.

The XPS valence-band region of $GdScO_3$ also consists of eight features, a–h. The four features close to the Fermi level are a, b, c, and d at −4.0, −5.5, −7.5, and −8.5 eV. The O 2p states are located from −3 to −5.5 eV (a and b), while the Gd 4f states are relatively localized from −7.5 to −8.5 eV (c and d). Features e and f are located at −20.0 and −22.0 eV, followed by relatively small feature g at −26.5 eV. The O 2s states are at around −22 eV, and the Gd 5p multiplet reaches from −18 to −26 eV. Sc 3p feature h takes place at −30.5 eV. Features a–d close to the Fermi level are in very good agreement with both calculations. The intensities of features e and f are reversed in the calculation with respect to experiment, whereas the g and h features are reproduced well.

Finally the XPS valence-band $DyScO_3$ consists of nine features, a–i. Features a, b, and c are located at −4.5, −7.0, and −9.0 eV, followed by a shoulder at −13.0 eV (d). From −3 to −5 eV the O 2p states take place. The Dy 4f multiplet is comprised of features b, c, and d. Features e, f, and g take place at −18.5, −20.5, and −23.0 eV. O 2s states are located at around −22 eV. Sc 3p feature i at −30.5 eV has prepeak h at −27.5 eV. The Dy 5p multiplet reaches from −18.5 to −27.5 eV. The three features a, b, and c near the Fermi level are reproduced by the calculation with U=0.8 Ry a little bit too far away from the Fermi level, but the calculation with U=0.4 Ry is in perfect agreement. Multiplet feature d is missing in calculations. Features e, f, and g are calculated as two separated peaks. Feature i and prepeak h are in very good agreement with the calculation. In general the shape of the XPS measurement is reproduced by the calculations in a satisfactory way. However, there are some differences in detail. The comparison for $GdScO_3$ and $DyScO_3$ shows a difference at the group of features around −20 eV. The com-

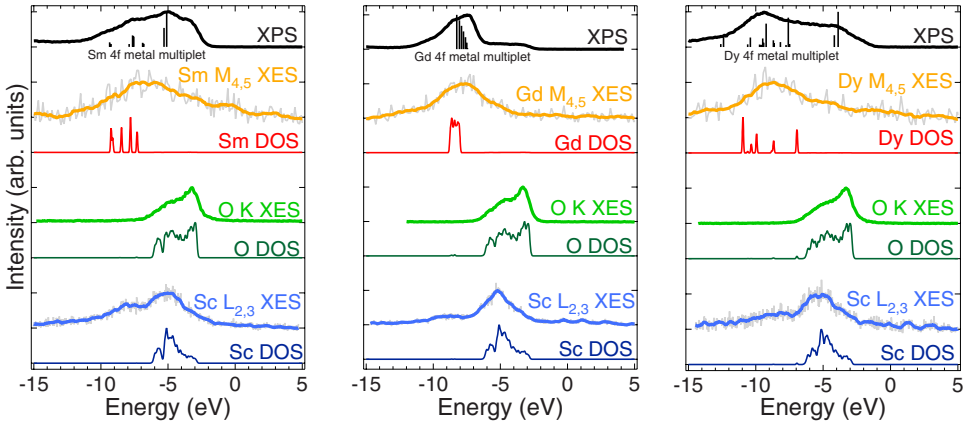

FIG. 5. (Color online) XPS valence bands and experimental R $M_{4,5}$, O K, and Sc $L_{2,3}$ XE spectra (thick lines). The corresponding calculated partial DOSs (thin lines) are also shown and are shifted by −2.5 eV for comparison with experiment. Calculations of R metals in the Russel-Saunders spin-orbit coupling scheme from Lang *et al.*[38] are plotted below the $RScO_3$ XPS spectra.

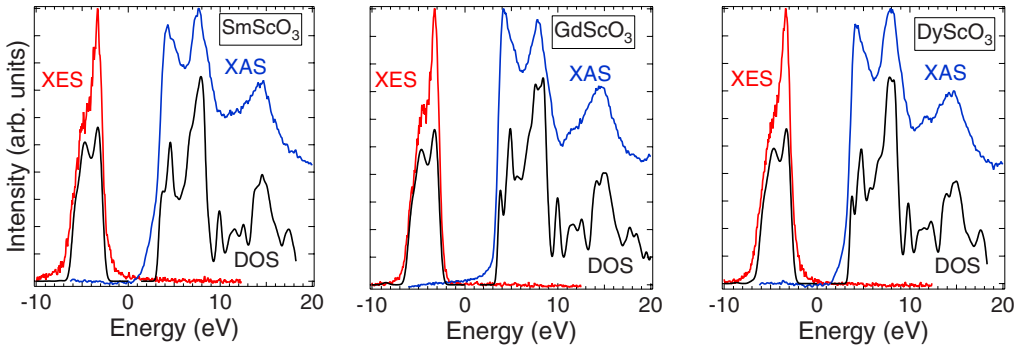

FIG. 6. (Color online) O*K* XAS (blue) and XES (red) of $SmScO_3$, $GdScO_3$, and $DyScO_3$. LDA+*U* calculations below experimental data were convoluted with 0.7 (XES) and 0.4 eV (XAS) Gaussian for experimental broadening. The calculated unoccupied states are shifted upwards by 1.4 eV for $SmScO_3$, 1.6 eV for $GdScO_3$, and 1.5 eV for $DyScO_3$.

parison of the states closer to the Fermi level reveals differences for $SmScO_3$ by rendering the rare-earth 4*f* multiplet in position and splitting. Also the $DyScO_3$ calculations with $U=0.8$ Ry show the 4*f* states shifted away from the Fermi level. The position of the rare-earth 4*f* states is influenced by the choice of the *U* parameter. Other differences arise from the fact that the calculations did not include multiplet effects which are more important for rare-earth atoms than for oxygen and scandium atoms.

Now we turn to a detailed comparison between XPS valence-band, XES, and pDOS of the calculations. In the left panel of Fig. 5 the XE spectra of Sm $M_{4,5}$, O *K*, and Sc $L_{2,3}$ are displayed with corresponding partial DOS from the GGA+*U* calculations. Below the XPS valence-band spectra of $RScO_3$, the rare-earth 4*f* multiplet calculations of Lang *et al.*[38] are plotted. These calculations are using the Russel-Saunders spin-orbit coupling scheme for comparison with XPS valence-band spectra of trivalent rare-earth metals. Comparable calculations were done by Gerken.[39] The XE spectra have been plotted on a common energy scale with the XPS valence band by using corresponding XPS core level binding energies for calibration (Sm 3*d*: 1109.5 eV; O 1*s*: 530.0 eV; and Sc 2*p*: 401.5 eV). The $M_{4,5}$ XE spectrum consists of Sm 4*f* features from −2 to −11 eV with a maximum at −6 eV. The calculated partial DOS has four features from −7 to −10 eV. This multiplet structure is better rendered by the multiplet calculation of trivalent Sm 4*f* states, which also shows the main peak at −5 eV.

The O *K* XE spectrum has two features at −3.0 and −5.0 eV. These features agree with the calculated O 2*p* states. The −5.0 eV feature is due to hybridization of O 2*p* and Sc 3*d* levels. The Sc $L_{2,3}$ XE spectrum is comprised of three features at −3.0, −5.0, and −8.0 eV. The −3.0 eV is due to the hybridization between O 2*p* and Sc 3*d*, and the −5 eV feature is the main feature of Sc 3*d* levels. The third feature at −8.0 eV is not covered by the calculation because it is due to the spin-orbit splitting of Sc 2*p* of ~4 eV. But this cannot completely explain the shape and energetic position of this feature. It is not clear if there is another feature due to an interaction between Sc and Sm which might be a *d* state coupling that was formerly found for complex oxides.[7,8,32]

Also the XE spectra of $GdScO_3$ are compared with the XPS valence-band and pDOS calculations (Fig. 5, middle panel). The calculation of trivalent Gd 4*f* multiplets from Lang *et al.*[38] is plotted below the XPS valence-band spectrum. XPS core level energies have been used to get a common energy scale (Gd 3*d*: 1189.5 eV; O 1*s*: 530.0 eV; and Sc 2*p*: 401.5 eV). The Gd $M_{4,5}$ XE spectra are comprised of an intense feature at −8.0 eV with a shoulder at −6.0 eV. The main feature is rendered by the band-structure calculation as Gd 4*f* states. This is also in comparison with the multiplet calculation of trivalent Gd 4*f* states. The O *K* XES has a O 2*p* main feature at −3.5 eV with a shoulder at −5.0 eV which is due to hybridization between O 2*p* and Sc 3*d*. The calculations show O 2*p* levels around −5 eV. The Sc $L_{2,3}$ XE spectrum consists of three features: a Sc 3*d* feature at −5.0 eV with a shoulder at −3.5 eV, which is due to hybridization between Sc 3*d* and O 2*p*, and a small shoulder from −7.5 to −10 eV which is due to spin-orbit splitting of the Sc 2*p*(~4 eV). As discussed before an interaction between Sc and Gd is possible but weaker than for $SmScO_3$. The calculation shows the Sc 3*d* features at −3.5 and −5.0 eV, but the feature around −9 eV is missing.

In the right panel of Fig. 5 the XES experiments of $DyScO_3$ are shown, along with the band-structure-calculated partial densities of states. The common energy scale is achieved by use of the XPS core level energies (Dy 3*d*: 1296.0 eV; O 1*s*: 530.0 eV; and Sc 2*p*: 401.5 eV). Multiplet calculations of trivalent Dy 4*f* states[38] are plotted below the XPS VB spectrum. The Dy $M_{4,5}$ XE spectra are comprised of four Dy 4*f* features at −5.0, −7.0, −9.0, and −13.0 eV. The three features from −5.0 to −9.0 eV are calculated with lower energy, and the feature at −13.0 eV is missing in the calculation which is due to not included multiplet effects. In the O *K* XE spectrum the O 2*p* main feature at −3.5 eV with a Sc 3*d* hybridization shoulder from −5.0 to −7.0 eV is in perfect agreement with the calculation. The Sc $L_{2,3}$ spectrum consists of a peak at −5.0 eV with a shoulder at −3.5 eV and a smaller peak at −8.0 eV. As discussed for the other samples the −8.0 eV peak is due to the spin-orbit splitting of Sc 2*p*. The interaction between Sc and Dy might be smaller than for $SmScO_3$ but larger than for $GdScO_3$. The calculation renders the peaks at −3.5 and −5.0 eV.

Apart from the appearance of *R* 4*f* states, the electronic structures of $SmScO_3$, $GdScO_3$, and $DyScO_3$ are very similar. The 4*f* levels, dominating the valence band, are located at −7.5 eV for Gd. For the Sm and the Dy compounds the

R 4*f* levels are more multiplet splitted in the range from −6 to −10 eV for Sm and from −5 to −9 eV for Dy. The band-structure calculations show some difference to the *R* 4*f* states due to multiplet splitting of 4*f* states. This is visible by comparing multiplet calculations for trivalent rare-earth 4*f* states with the experimental data.

The O and Sc states for which multiplet splitting is less important are in good agreement with the band-structure calculations. At around −5 eV there are O 2*p* states which are hybridized with Sc 3*d*. An interaction between Sc and *R* atoms might be present in the Sc $L_{2,3}$ XE spectra at around −8 eV. Such a hybridization was found for $DyScO_3$ and $GdScO_3$ by Lucovsky *et al.*[7] and for $AScO_3$ perovskite alloys by Halilov *et al.*[40]

Now we want to discuss the unoccupied states with help of O 1*s* x-ray absorption (XA) spectra and calculated O pDOS convoluted with a 0.4 eV Gaussian for experimental broadening (Fig. 6). The XA spectra are shifted by the binding energy of the O 1*s* XPS peak (530 eV) for comparison with the calculations. In the range of 1–20 eV unoccupied Sc 3*d* states and *R* 5*d* states hybridized via oxygen are present.[7] Three intense features are assigned to Sc 3*d* at 4 eV, Dy 5*d* at 14 eV, and a Sc *R* mixed *d* state at 7.5 eV. At 5 and 11 eV smaller features are visible which are due to splitting of the main features by an uniaxial crystal distortion.

Finally we want to determine the band gaps of the samples by combining the O 1*s* XA spectra and the O *K* XE spectra (Fig. 6). The DOS from the first-principles calculations is also shown for comparison. There are different methods in literature to obtain band gaps which are comparable with the method that is used here. Very similar is the approach made by Dong *et al.*,[41] where the onset of the O 1*s* XAS and O *K* edge XES peaks was taken to determine the band gap of ZnO. Another possibility is given by Hüfner *et al.*[42] where the band gap of NiO is determined between Fermi level of XPS and maximum of the first peak of a bremsstrahlung isochromat spectroscopy (BIS) spectrum. The advantages of XAS and XES compared with band-structure calculations are that a small density of states at the edge of the band gap are taken into account, the experiments are made under very similar conditions in a short time range, and the precise relative calibration of XAS and XES. A disadvantage is the element-specific band gap, but due to the delocalization of the O 2*p* electrons this method is applicable.

As the band gap is formed by rare-earth 4*f*, 5*d*, and scandium 3*d* states hybridized with O 2*p*, the LDA+*U* correction "naturally" increases the band gap, as is known from many *ab initio* studies of correlated oxides. The values of band gaps resulting from band-structure calculations should not be taken too seriously because of empirical adjustment of the *U* value. Still, it is comfortable, having proceeded from, primarily, the adjustment of the 4*f* peak positions in the XP spectra, to arrive at values for the band gaps which are in the range of the results from optical experiments. Also the shape of the calculations is in very good agreement with the shape of the XAS and XES experiments. This yields the conviction that the overall description of the underlying band structure is correct.

In Fig. 6 the band gap of the calculations is enlarged by shifting the unoccupied states (1.4 eV for $SmScO_3$, 1.6 eV for $GdScO_3$, and 1.5 eV for $DyScO_3$) to achieve perfect agreement with the XA spectra and the XE spectra. To determine the band gap in the experiment the highest occupied and the lowest unoccupied states of the enlarged calculations are used so one can overcome the too small band gap of the calculations. The calculated and experimental values are compared with ultraviolet absorption results,[18] ellipsometry measurements,[7,43] and a combination of internal photoemission and photoconductivity measurements[19] in Table I. The values determined by XAS and XES are slightly higher than the results from UV spectroscopy from Cicerella,[18] but the agreement with Lucovsky *et al.*[7] and Afanas'ev *et al.*[19] is very good. Ellipsometry measurements of Lim *et al.*[43] for $GdScO_3$ give higher results for the band gap than other methods, while the transmission spectrum in the same paper show the absorption onset below 6 eV, which is in agreement with the present results.

TABLE I. Band gaps of rare-earth scandates from this work (LDA+*U*; experiment) in comparison with values from literature.

	$SmScO_3$ (eV)	$GdScO_3$ (eV)	$DyScO_3$ (eV)
Cicerella (Ref. 18)	5.4	5.2	5.3
Lim *et al.* (Ref. 43)	5.5–6.0	6.5	
Afanas'ev *et al.* (Ref. 19)		5.6	5.7
Lucovsky *et al.* (Ref. 7)		5.8	
LDA+*U*	4.2	4.2	4.4
experiment	5.6	5.8	5.9

This partly different results can be understood if one takes into account the differences of the techniques and their interpretation. The band gap is defined as the energetic difference between the highest occupied and the lowest unoccupied level in the ground state. In experiments the initial state is usually the ground state, while the final state differs for various techniques. For XPS and XES the final state is a *N*-1 electron state where one electron has left the atom. During the XAS process the electron stays in the atom and the final state is a *N* electron state. A different charge of the final states in XPS and XAS processes implies a need to introduce a correction in order to permit a superposition of both in the common energy scale. The correction becomes larger the more "dense" the core states are. Consequently the difference (correction) is large in *R* 4*f* but negligible in O 2*p* (weak localization) and in Sc 3*d* (empty *d* shell), the states which essentially flank the band gap.

IV. CONCLUSIONS

In conclusion the electronic structure of $SmScO_3$, $GdScO_3$, and $DyScO_3$ is investigated with XPS, XAS, XES, and band-structure calculations (WIEN2K). Magnetism versus temperature measurements reveal antiferromagnetic coupling at 2.96 ($SmScO_3$), 2.61 ($GdScO_3$), and 3.10 K ($DyScO_3$). For $DyScO_3$ a Rietveld refinement of a 2 K neutron-diffraction data set gives a spin arrangement of Dy in the

Pbnm structure (Shubnikov group: $Pb'n'm'$). The XPS valence band is dominated by the R 4f multiplet structure corresponding to a trivalent state. XES measurements show that the oxygen 2p and Sc 3d levels are strongly hybridized. The rare-earth 5d states may contribute slightly to this hybridization. The band gaps of the compounds are determined by combining XES and XAS measurements. For $SmScO_3$, $GdScO_3$, and $DyScO_3$ the band gaps were 5.6, 5.8, and 5.9 eV, respectively.

ACKNOWLEDGMENTS

Part of this work has been performed at the Advanced Light Source (ALS), Lawrence Berkeley National Laboratory, Berkeley, USA, which is operated under Contract No. DE-AC03-76SF00098. M.R. gratefully acknowledges financial support from the GRK695: Nonlinearities of optical materials. Financial support by the Ph.D. program (Lower Saxony) is gratefully acknowledged by M.P.

*mraekers@uos.de

†Present address: University of Ulm, Institut für Festkörperphysik, Albert-Einstein-Allee 11, D-89069 Ulm, Germany. karsten.kuepper@uni-ulm.de

‡mneumann@uos.de

[1] S. Maekawa, T. Tohyama, S. E. Barnes, S. Ishihara, and W. K. Khaliullin, *Physics of Transition Metal Oxides* (Springer, Berlin, 2004).

[2] R. von Helmolt, J. Wecker, B. Holzapfel, L. Schultz, and K. Samwer, Phys. Rev. Lett. **71**, 2331 (1993).

[3] S. Jin, T. H. Tiefel, M. McCormack, R. A. Fastnacht, and R. R. H. Chen, Science **264**, 413 (1994).

[4] M. Dawber, K. M. Rabe, and J. F. Scott, Rev. Mod. Phys. **77**, 1083 (2005).

[5] H. Fu and R. E. Cohen, Nature (London) **403**, 281 (2000).

[6] K. J. Choi *et al.*, Science **306**, 1005 (2004).

[7] G. Lucovsky, J. G. Hong, C. C. Fulton, Y. Zou, R. J. Nemanich, H. Ade, D. G. Scholm, and J. L. Freeouf, Phys. Status Solidi B **241**, 2221 (2004).

[8] G. D. Wilk, R. M. Wallace, and J. M. Anthony, J. Appl. Phys. **89**, 5243 (2001).

[9] C. Zhao *et al.*, Appl. Phys. Lett. **86**, 132903 (2005).

[10] K. H. Kim, D. B. Farmer, J.-S. M. Lehn, P. Venkateswara Rao, and R. G. Gordon, Appl. Phys. Lett. **89**, 133512 (2006).

[11] J. Schubert, O. Trithaveesak, A. Petraru, C. L. Jia, R. Uecker, P. Reiche, and D. G. Schlom, Appl. Phys. Lett. **82**, 3460 (2003).

[12] J. H. Haeni *et al.*, Nature (London) **430**, 758 (2004).

[13] G. Catalan, A. Janssens, G. Rispens, S. Csiszar, O. Seeck, G. Rijnders, D. H. A. Blank, and B. Noheda, Phys. Rev. Lett. **96**, 127602 (2006).

[14] P. Kužel, F. Kadlec, J. Petzelt, J. Schubert, and G. Panaitov, Appl. Phys. Lett. **91**, 232911 (2007).

[15] J. L. F. Da Silva, M. V. Ganduglia-Pirovano, J. Sauer, V. Bayer, and G. Kresse, Phys. Rev. B **75**, 045121 (2007).

[16] D. I. Bilc, R. Orlando, R. Shaltaf, G.-M. Rignanese, J. Íñiguez, and P. Ghosez, Phys. Rev. B **77**, 165107 (2008).

[17] P. Delugas, V. Fiorentini, A. Filippetti, and G. Pourtois, Phys. Rev. B **75**, 115126 (2007).

[18] E. Cicerella, Ph.D. thesis, OGI School of Science & Engineering at Oregon Health & Science University, 2006.

[19] V. V. Afanas'ev, A. Stesmans, C. Zhao, M. Caymax, T. Heeg, J. Schubert, Y. Jia, D. G. Schlom, and G. Lucovsky, Appl. Phys. Lett. **85**, 5917 (2004).

[20] A. Moewes, A. V. Postnikov, B. Schneider, E. Z. Kurmaev, M. Matteucci, V. M. Cherkashenko, D. Hartmann, H. Hesse, and M. Neumann, Phys. Rev. B **60**, 4422 (1999).

[21] K. Kuepper, A. V. Postnikov, A. Moewes, B. Schneider, M. Matteucci, H. Hesse, and M. Neumann, J. Phys.: Condens. Matter **16**, 8213 (2004).

[22] K. Kuepper, B. Schneider, V. Caciuc, M. Neumann, A. V. Postnikov, A. Ruediger, A. A. Grabar, and Y. M. Vysochanskii, Phys. Rev. B **67**, 115101 (2003).

[23] R. Uecker, B. Velickov, D. Klimm, R. Bertam, M. Bernhagen, M. Rabe, M. Albrecht, R. Fornan, and D. G. Schlom, J. Cryst. Growth **310**, 2649 (2008).

[24] J. J. Jia *et al.*, Rev. Sci. Instrum. **66**, 1394 (1995).

[25] A. C. Larson and R. B. Von Dreele, *GSAS: General Structural Analysis System* (LANSCE, Los Alamos National Laboratory, Los Alamos, NM, 1994).

[26] D. J. Singh, *Planewaves, Pseudopotentials and the LAPW Method* (Kluwer Academic, Boston, 1994).

[27] P. Blaha, K. Schwarz, G. K. H. Madsen, D. Kvasnicka, and J. Luitz, *An Augmented Plane Wave + Local Orbitals Program for Calculating Crystal Properties* (Karlheinz Schwarz, Techn. Universität Wien, Austria, 2001).

[28] J. P. Perdew, K. Burke, and M. Ernzerhof, Phys. Rev. Lett. **77**, 3865 (1996).

[29] J. P. Perdew, K. Burke, and M. Ernzerhof, Phys. Rev. Lett. **78**, 1396 (1997) Erratum.

[30] V. I. Anisimov, F. Arysetiawan, and A. I. Lichtenstein, J. Phys.: Condens. Mat. **9**, 767 (1997).

[31] V. I. Anisimov and O. Gunnarsson, Phys. Rev. B **43**, 7570 (1991).

[32] R. P. Liferovich and R. H. Mitchell, J. Solid State Chem. **177**, 2188 (2004).

[33] H. Bonrath, K. H. Heliwege, K. Nicolay, and G. Weber, Phys. Kondens. Mater. **4**, 382 (1966).

[34] G. R. Stewart, J. A. Barclay, and W. A. Steyert, Solid State Commun. **29**, 17 (1979).

[35] E. F. Bertaut, Acta Crystallogr., Sect. A: Cryst. Phys., Diffr., Theor. Gen. Crystallogr. **24**, 217 (1968).

[36] P. Larson, W. R. L. Lambrecht, A. Chantis, and M. van Schilfgaarde, Phys. Rev. B **75**, 045114 (2007).

[37] J. H. Scofield, J. Electron Spectrosc. Relat. Phenom. **8**, 129 (1976).

[38] J. K. Lang, Y. Baer, and P. A. Cox, J. Phys. F: Met. Phys. **11**, 121 (1981).

[39] F. Gerken, J. Phys. F: Met. Phys. **13**, 703 (1983).

[40] S. V. Halilov, M. Fornari, and D. J. Singh, Phys. Rev. B **69**, 174107 (2004).

[41] C. L. Dong, C. Persson, L. Vayssieres, A. Augustsson, T. Schmitt, M. Mattesini, R. Ahuja, C. L. Chang, and J.-H. Guo, Phys. Rev. B **70**, 195325 (2004).
[42] S. Hüfner, P. Steiner, I. Sander, M. Neumann, and S. Witzel, Z. Phys. B: Condens. Matter **83**, 185 (1991).
[43] S.-G. Lim, S. Kriventsov, T. N. Jackson, J. H. Haeni, D. G. Schlom, A. M. Balbashov, R. Uecker, P. Reiche, J. L. Freeouf, and G. Lucovsky, J. Appl. Phys. **91**, 4500 (2002).